RSC Advances




ROYAL SOCIETY OF CHEMISTRY

www.rsc.org/advances

Ceramics Research Laboratory
3-101-1,Honmachi, Tajimi, Gifu 507-0033,JAPAN TEL +81-572-24-8110 FAX +81-572-24-8109

# Table of contents

The convenient characterization method of the nanostructural hydrated porous ceramic body using a hydrophilic ionic liquid is established.

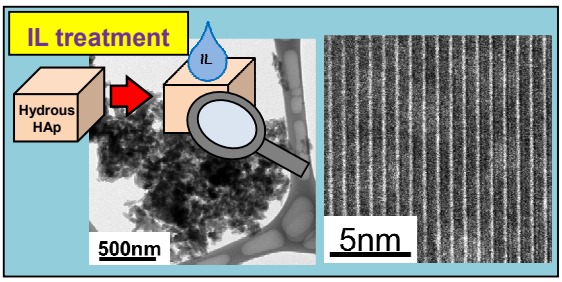

Journal Name

RSCPublishing

ARTICLE

# Solvent effect on observation of nanostructural hydrated porous ceramic green bodies using hydrophilic ionic liquid

Cite this: DOI: 10.1039/x0xx00000x

Received ooth January 2012,
Accepted ooth January 2012

DOI: 10.1039/x0xx00000x

www.rsc.org/

Chisato Takahashi, Deepak K. Pattanayak, Takashi Shirai and Masayoshi Fuji*

Structural observation of hydrated porous hydroxyapatite (HAp) during its processing was observed in presence of a hydrophilic ionic liquid using transmission electron microscopy (TEM). The images showed the nanostructure of the hydrated HAp green body. Furthermore, in order to optimize the nanostructural observations of the HAp green ceramics, various solvent effects were investigated. In addition, the shrinkage behavior of the structural porous HAp ceramic green body with respect to humidity was revealed. The as-prepared sample showed particles approximately 20-150 nm in diameter, which gradually contracted to approximately 10-100 nm upon drying in a humidity chamber. Following sintering at 1000 ˚C, the pores had further contracted to approximately 100-500 nm. The dimensional change of the hydrous HAp was less than 1 %. These results suggest that the hydrous HAp can maintain its nanostructure after the IL treatment. This technique would be useful for the structural characterization of wet ceramics. The nano-scaled characterization of the hydrous green body can provide valuable information for the fabrication of advanced ceramic materials.

## 1. Introduction

Porous ceramic materials are fabricated by various methods, such as, the impregnation of polymeric sponges, gelcasting of foam, extrusion and automated manufacturing processes.[1-4] Janney and co-workers reported the gelcasting process which is used to fabricate samples with complex geometries as well as high mechanical strength ceramic bodies.[5,6] Using this method, various types of ceramics, such as alumina,[7,8] silicon nitride,[9] rutile,[10] silicon carbide,[11,12] and alumina–zirconia composites, have been developed.[13] Following the solidification step, when this method is further combined with foamed suspensions by in situ polymerization, it can be used to form an internally cross-linked network that transforms the foam into a gelled body with the ability to bear a load.[14,15] The gelled body is then sintered to fabricate the desired materials that can be used in various functional applications.

In general, the main structure of the HAp ceramics is defined by the humidity process. Thus, it is essential to reveal the nano-structure of the hydrous HAp green body during the humidity process in order to enhance the fabrication process of the ceramics. However, the fine structure of the green body is difficult to observe using an electron microscope due to its hygroscopic nature.

Recently, room-temperature ionic liquids (RTILs) have been reported as organic fused salts that consist of cations and anions and remained as fluid below 100 ˚C.[16,17] ILs are frequently used as a solvent in various chemical reactions,[18] syntheses,[19,20] electrolyte in batteries,[21] and dispersant,[22] etc. Due to their negligible vapor pressure and high conductivity, biological samples using the IL were observed using the electron microscope without the addition of a conductive coating.[23,24] In addition, Kuwabata et al. reported that the hydrated materials can be observed with the aid of a hydrophilic IL using a scanning electron microscope (SEM).[25,26] Based on our previous reports, the hydrated agar gel, seaweed swelled by water and an HAp porous green body have been successfully observed using a field emission scanning electron microscope (FE-SEM).[27-29] The FE-SEM observation mechanism using the hydrophilic IL was also proposed.[29] In the porous HAp green body case, the morphological change of the sample and the shrinkage behavior of the pores during the drying process were revealed by the FE-SEM. However, there has been no report to date about observations of the nanostructure of the hydrous ceramics using a general TEM. In addition, the solidification and calcination behavitors on a nanoscale of the hydrous HAp particles during the drying process have not been revealed. The thickness of the TEM sample needs to be thinner unlike the SEM sample. In our previous studies, we tried to confirm the crystal structure of the hydrous montmorillonite using our established method for the TEM observations.[30,31] We found that solvent needs to be used for the TEM sample preparation. However, there is a need to further develop the observation method using a TEM in order to apply this method to characterize a wide range of materials in various research

fields. Therefore, we focused on the structural change of the hydrous ceramics by the solvent effect.

In the present study, a simple method for TEM observations of the nanostructured hydrous HAp green body using a hydrophilic IL was attempted. In order to establish the TEM observation method, the solvent effect on the nanostructural hydrated HAp green body was confirmed. The shrinkage behaviors of the fine particles of the HAp during the drying process were observed with the aid of the present method by the TEM observation. In addition, the crystal structures of the hydrous HAp samples were confirmed by comparing the XRD and TEM-SAED results.

## 2. Experimental

### 2.1. Materials

For the gelcasting process, a hydroxyapatite (HAp) powder, dispersant, monomer and various initiators were used. The details of the materials, which were used for the fabrication of the HAp, have been described elsewhere.[28]

The ionic liquid; 1-butyl-3-methylimidazolium tetrafluoroborate ([BMIM][$BF_4$]) (Kanto Chem. Co., Japan) was used after drying in vacuum desiccators at 60 °C for 3 days. The water content of the IL was below 128 ppm, as measured by the Karl-Fischer titration method.

### 2.2. Methods

Figure S1 shows a schematic representation of the gel casting process used in this investigation. The detailed gel casting procedure has already been described elsewhere.[32] The water contents of both the as-prepared porous HAp green body and the specimens that had been stored in the humidity chamber were measured by Karl-Fischer titration (Kyoto Electronics Co., Japan. MKA-610). Each porous body was cut into the same 5.0 × 5.0 × 5.0 $mm^3$ size for this measurement.

The as-prepared sample and the sample stored in the humidity chamber from 90 to 50 % were both treated with the IL. The IL was prepared by adjusting its water content to 30 mol % (weight amount ratio; water : IL = 1 : 29.3) and was stored in a desiccator for 2 h. All these samples were subsequently maintained in a vacuum dryer for 24 h before being centrifuged for 5 min at 10,000 rpm to remove any excess IL. These samples were cut, then, subsequently dispersed in water (weight amount ratio; sample : water = 1 : 20) and skimmed off by a copper mesh with carbon-coated plastic microholes. In addition, the as-prepared sample was dispersed in ethanol in order to further establish the method (weight amount ratio; sample : ethanol = 1 : 20). These samples were observed using a TEM (JEM2010, JEOL Co., Japan) operated at 120 kV. For comparison, the porous HAp bodies were sintered at 1000 ºC for 2 h and dispersed in water and skimmed off by a copper mesh with carbon-coated plastic microholes. The sintering of the porous bodies was carried out at 1000 ºC for 2 h in an atmospheric furnace and the rate of heating was maintained at 1 ºC/min to avoid thermal cracking.

The X-ray diffraction (XRD) pattern (Ultima 5, Rigaku Co., Japan) of the hydroxyapatite powder was recorded in the 2θ range from 10 to 60° at the scan rate of 1° / min using Cu Kα radiation (λ = 0.1542 nm, 40 kV, 40 mA).

The size retention of the as-prepared porous HAp green bodies, the samples that were treated in the humidity chamber as it was reduced from 90 to 50% relative humidity, and those that were sintered at 1000 ºC for 2 h were all measured both before and after the IL treatment. In addition, the size retentions of the as-prepared porous HAp green bodies after the TEM sample preparation using the IL diluted by water or ethanol were measured. The dimensions of the samples were measured using a ruler. The method has been described elsewhere.[32] The size retention ratios were calculated (X × Y × Z / 125 × 100).

## 3. Results and discussion

### 3.1. Crystal structure of HAp as received and after sintering

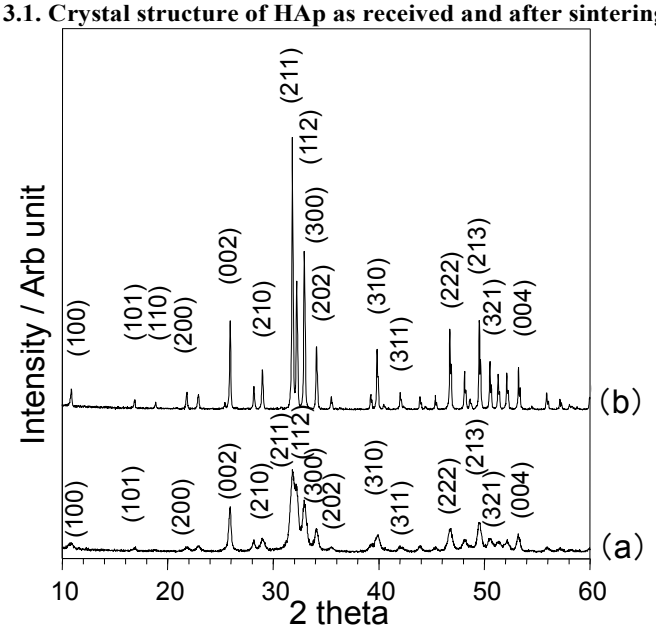


| (a) | | (b) | |
|---|---|---|---|
| 2θ (deg) | d (Å) | 2θ (deg) | d (Å) |
| 10.82 | 8.17 | 10.82 | 8.17 |
| 16.82 | 5.27 | 16.84 | 5.26 |
| 21.78 | 4.08 | 18.79 | 4.72 |
| 25.86 | 3.44 | 21.82 | 4.07 |
| 28.96 | 3.08 | 25.88 | 3.44 |
| 31.8 | 2.81 | 28.97 | 3.08 |
| 32.18 | 2.78 | 31.77 | 2.81 |
| 32.94 | 2.72 | 32.90 | 2.78 |
| 34.06 | 2.63 | 32.2 | 2.72 |
| 39.84 | 2.26 | 34.05 | 2.63 |
| 42.06 | 2.15 | 39.82 | 2.26 |
| 46.74 | 1.94 | 42.03 | 2.15 |
| 49.48 | 1.84 | 46.71 | 1.94 |
| 50.54 | 1.80 | 49.47 | 1.84 |
| 53.18 | 1.72 | 50.49 | 1.81 |
| | | 53.14 | 1.72 |

Fig. 1: XRD spectra of HAp (a) as received and (b) subjected to heat treatment at 1000ºC for 2h.

Figure 1 shows the XRD spectra of the HAp as received and after the gelcasting process + calcination at 1000 ºC for 2 h. It should be noted that the HAp as received means the raw powder in a dried condition. Figure 1a indicates that the powder contains a pure HAp phase, identified by the corresponding 2θ values. The diffractions confirmed that the (100), (101), (200), (002), (210), (211), (300) and (202) reflections at 8.17, 5.27, 4.08, 3.44, 3.08, 2.81, 2.78 and 2.63 Å, respectively, are a constituent of the HAp. In this study, we mainly focused on diffractions in order to compare with the TEM-SAED or First Fourier Transform (FFT) pattern. The HAp powder was

subsequently used for the gelcasting process in order to fabricate the porous HAp green body samples. Figure 1b indicates that the calcined HAp powder has additional peaks compared to Figure 1a. Focusing on the diffractions, the (100), (101), (110), (200), (002), (210), (211), (300) and (202) reflections at 8.17, 5.26, 4.72, 4.07, 3.44, 3.08, 2.81, 2.72 and 2.63 Å, respectively, are a constituent of the HAp. Most of the peaks are assigned to the HAp even after the gelcasting process + calcination at 1000 ºC for 2 h. Compared to Figure 1a, almost the same reflections were observed although the drying and calcination process have been carried out. These results suggest that the crystal structure of the HAp can be maintained during the fabrication process, although the peaks became much sharper.

### 3.2. Structural observation of a sintered HAp without any treatment

Figure 2 shows TEM images of a sintered porous HAp body without any treatment (Figures 2a-c) and its corresponding FFT pattern (Figure 2d). In the present study, the sintered HAp was measured for comparing the results with the hydrated HAp green bodies under different conditions. The low-magnification image shows that the sintered sample consists of well-facetted rock-like grains in the range of approximately 100-500 nm in diameter (Figure 2a). In addition, it is clear that the particles become bonded to each other during the sintering process. The high-magnification image, which is observed from the [010] direction, indicates a regularly-ordered structure (Figure 2c). A periodicity layer parallel to the (100) plane of the HAp crystal is 8.19 Å. From the FFT pattern corresponding to Figure 2c, the d-spacings were obtained for the (100), (001), (101) and (300) reflections at 8.24, 6.92, 5.26 Å and 2.78 Å, respectively.

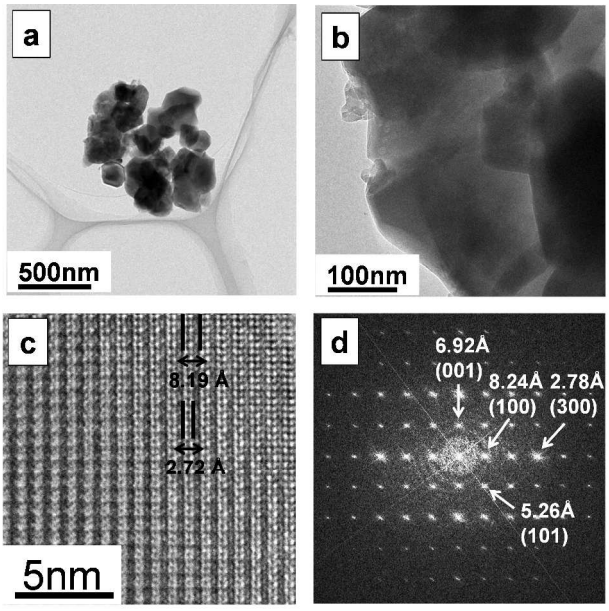


Fig. 2: TEM images of the porous HAp green body sintered at 1000ºC for 2h following osmium coating (a), (b) bright-field image, (c) high-resolution image and (d) FFT pattern.

The marked layers in Figure 2c correspond to the (100) and (300) reflections. These results are in good agreement with the XRD results as seen in Figure 1. In this study, the XRD peak derived from the (001) reflection was not obtained.

### 3.3. Structural observation of as-prepared HAp treated with IL

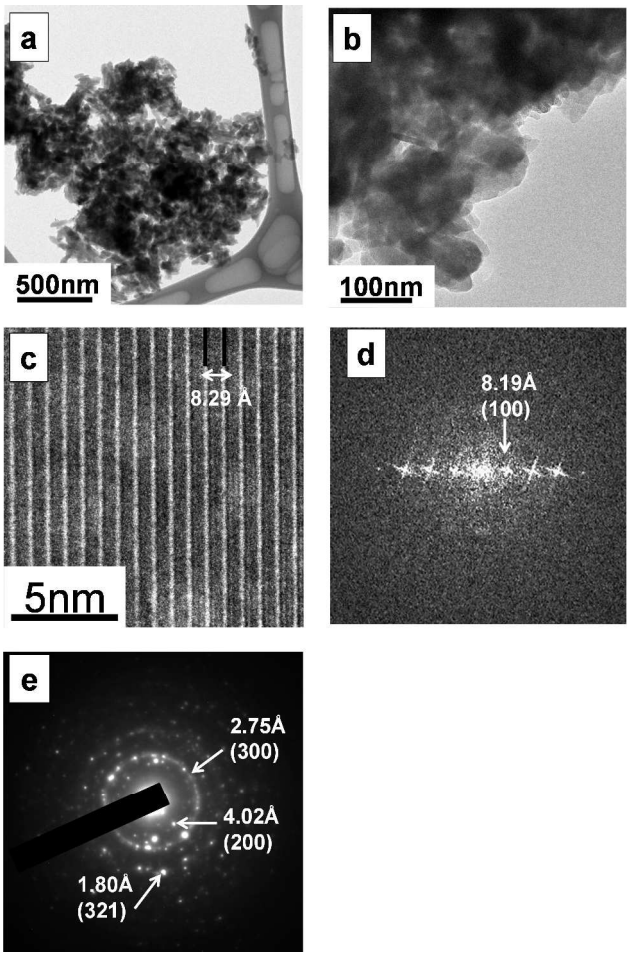


Fig. 3: TEM images of the as-prepared porous HAp green body following the IL treatment using water (a), (b) bright-field image, (c) high-resolution image, (d) FFT pattern and (e) SAED pattern.

Figure 3 shows TEM images of an as-prepared hydrous HAp green body after the IL treatment in the presence of water (Figure 3a-c) and its corresponding FFT pattern (Figure 3d) and SAED pattern (Figure 3e). In this measurement, the water was chosen as a diluted solution for the IL. The low-magnification image shows that the as-prepared hydrous HAp consisted of fine particles (Figure 3a). The sizes of the HAp particles are in the range of approximately 20-150 nm in diameter (Figure 3b). The high magnification image indicates a structure which is regularly-arranged (Figure 3c). A layer parallel to the (100) plane of the HAp crystal is 8.29 Å, similar to Figure 2c. The (100) reflection at 8.19 Å was obtained from the FFT pattern corresponding to Figure 3c (Figure 3d). The marked layer in Figure 3c corresponds to the (100) reflection. From the SAED pattern corresponding to Figure 3b, the d-spacing was mainly indexed (Figure 3e). The d-spacings obtained for the (200),

(300) and (321) reflections were 4.02, 2.75 and 1.80 Å, respectively. These results are in good agreement with the XRD results. Basically, the crystal structure of the as-preparaed HAp was maintained throughout the TEM observation with the aid of the IL treatment. Compared to the sintered HAp, small size particles were observed. This is due to the fact that each particle exists as individuals without bonding together. The swelled structure that maintained its hydrous condition using a TEM was successfully observed. Due to the high ion conductivity of the IL, no conductive coating is a necessary for the TEM observation. Furthermore, the crystal structure of the as-prepared HAp was able to be maintained in the TEM chamber under a high vacuum condition ($>2.0\times10^{-5}$ Pa). In order to understand the solidification behavior of the nanostructured HAp during the drying process, the structure of the HAp green body that had been stored in the humidity chamber in which the humidity was gradually reduced from 90 to 50 % was subsequently observed by TEM.

### 3.4. Structural observation of HAp that has been stored in a humidity chamber from 90 to 50 % after IL treatment

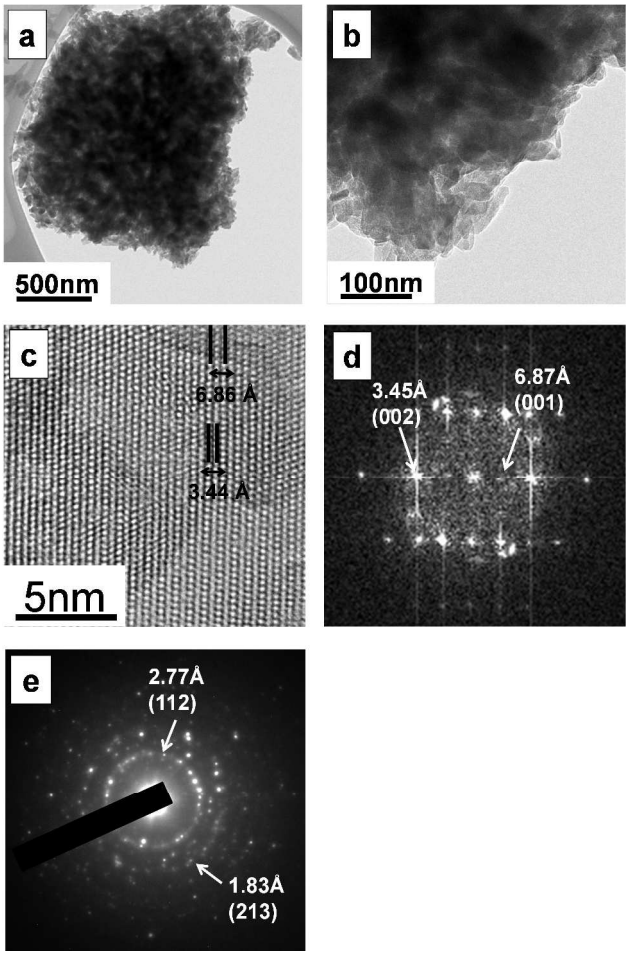


Fig. 4: TEM images of the HAp green body that has been stored in a humidity humid chamber at 90 to 50 % following the IL treatment using water (a), (b) bright-field image, (c) high-resolution image, (d) FFT pattern and (e) SAED pattern.

Figure 4 shows TEM images of a porous HAp green body that had been stored in the humidity chamber from 90 to 50 % after the IL treatment using water (Figure 4a-c) and its corresponding FFT pattern (Figure 4d) and SAED pattern (Figure 4e). The low-magnification image shows a porous HAp green body that had been stored in the humidity chamber from 90 to 50 % consisting of fine particles (Figure 4a). The size of the HAp particles are in the range of approximately 10100 nm in diameter (Figure 4b, S2). The high magnification image indicates the structure image which is regularly-structured similar to Figure 3c (Figure 4c). From the FFT pattern obtained from Figure 4c, a layer parallel to the (001) plane of the HAp crystal is 6.87 Å. Moreover, it was confirmed that a layer parallel to the (002) plane is 3.45 Å. It is explained that both layers correspond to the (001) and (002) reflections, respectively. From the SAED pattern corresponding to Figure 4b, the d-spacing was mainly indexed. The d-spacings were obtained for the (112) and (213) reflections as 2.77 and 1.83 Å, respectively. These results are in good agreement with the XRD results. Even in the present condition, the crystal structure image of the HAp was obtained. Compared to the as-prepared HAp green body, the particles sizes had decreased from approximately 20-150 to 10-100 nm. The size of the particles was clearly reduced following the drying process. It was caused by the evaporation of water within the HAp green body during the drying process. Based on these results, it was clear that the IL allows the structure of the HAp to be maintained under various hydrous conditions. We have tried to observe the HAp porous green bodies under various hydrous conditions. However, the sample preparation for the TEM observation needs to be developed. In order to evaluate the sample preparation, we need to observe the structure of the HAp porous green body treated with the IL using another diluted solution.

### 3.5. The effect of solvent on structural observation of hydrous HAp

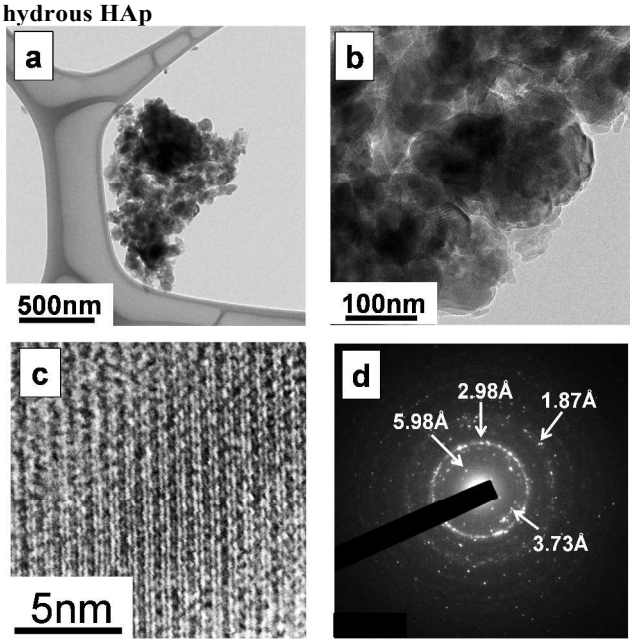


Fig. 5: TEM images of the as-prepared porous HAp green body following the IL treatment using ethanol (a), (b) bright-field image, (c) high-resolution image and (d) SAED pattern.

Figure 5 shows TEM images of an as-prepared hydrous HAp green body after the IL treatment using ethanol (Figures 5a-c) and its corresponding SAED pattern (Figure 5d). In this measurement, the ethanol was chosen for the dilution of the IL. The low-magnification image shows that the as-prepared hydrous HAp consisted of small agglomerations (Figure 5a). The size of the HAp particles is in the range of approximately 30-300 nm in diameter (Figure 5b). Compared to the HAp green body treated with the IL solution using water, the sizes of the particles had increased and the shapes of the particles were significantly different. The high-magnification image indicates the structure image which is non-regularly structured unlike Figure 3c (Figure 5c). Deformation of the crystal structure was clearly observed. From the SAED pattern corresponding to Figure 5b, each d-spacing was calculated. The values of 5.98, 3.73, 2.98 and 1.87 Å were obtained. These d-spacing values were different from the XRD results. It is considered that this difference was caused by the deformation of the crystal structure (Figure 5, S3).

We tried to observe the structures of the HAp porous green bodies under various hydrous conditions with the aid of ILs using a TEM. From the high resolution observations, the crystal structures of the hydrous HAp porous green bodies were clearly observed. It was found that the structures of the hydrous HAp porous green bodies were affected by the kind of diluted solution for the IL used in the TEM sample preparation. In fact, the structure of the hydrous HAp porous green body was significantly changed by the sample preparation using ethanol. The SAED pattern of the hydrous HAp green body was also changed due to the deformation of the crystal structure. These results showed that water is suitable for the IL dilution used in the TEM sample preparation.

From a previous study, we observed the morphology of the sintered HAp green body and the HAp green bodies in different hydrous conditions using a FE-SEM.[28] Compared to the FE-SEM images of the sintered HAp, the sizes of the HAp particles observed using a TEM are almost similar. In the case of the hydrous HAp green bodies that had been stored in the humidity chamber at 90 to 50 %, the SEM and TEM images are not comparable due to the limitation of the SEM observation using the IL. However, similar shrinkage of the hydrous HAp green bodies was observed by both techniques. Therefore, the water contents and volume shrinkage of the HAp porous green bodies after the TEM sample preparation need to be measured.

### 3.6. Size retention of HAp by IL treatment

Table 1. Comparison of the water contents of the porous HAp green bodies just after removal from the mold and of the samples maintained in the humidity chamber at 50 % relative humidity and of the porous body sintered at 1000ºC for 2h.

| Condition | As-prepared | 50 % | After sintering, 1000 ºC, 2 h |
|---|---|---|---|
| Size retention until sintering (%) | 100.0 | 77.1 | 50.7 |
| Size retention after IL treatment (%) | 99.0 | 99.4 | 99.8 |

Table 1 shows the water content of both porous HAp green bodies immediately after their removal from the mold, and of those kept in the humidity chamber from 90 to 50 % relative humidity and of the porous body sintered at 1000 ºC for 2 h. In this study, the water contents of each porous HAp green body used in the characterization was measured as a basic study for comparison. The water contents of the as-prepared porous HAp green body was 32.7 wt %. The water content of the samples dried at 50 % relative humidity was 13.5 wt %. These values are in good agreement with our previous work.[28,32] The porous HAp body sintered at 1000 ºC for 2 h had no water. We have already explained the details of this phenomenon in the previous studies.[32]

Table 2. Dimensional changes in the porous HAp green bodies just after removal from the mold and of the samples treated in the humidity chamber at 50 % relative humidity and of the porous body sintered at 1000ºC for 2h followed by examination of the size retention of the green bodies fabricated under similar conditions and subjected to the IL treatment.

| Condition | As-prepared | 50 % | After sintering, 1000 ºC, 2 h |
|---|---|---|---|
| Water content (Wt %) | 32.7 | 13.5 | - |

Table 2 shows the dimensional changes of the porous HAp green bodies just after removal from the mold, of the samples treated in the humidity chamber at 50 % relative humidity and of the porous body sintered at 1000ºC for 2h before and after the IL treatment. The size retention of the porous HAp green body was 77.1% during drying and 50.7 % after sintering at 1000 ºC for 2 h (Table 2). Table 2 shows that an approximately 20 % volume shrinkage occurred during the course of drying the green HAp porous bodies. From the results of Tables 1 and 2, it was confirmed that a 20% volume decrease of the HAp porous green body occurred due to the evaporation of the water during drying process. After the IL treatment of each HAp porous body, only less than a 1% shrinkage was observed. These results are in good agreement with our previous study.[32] However, in the present study, we used ethanol or water as a diluted solution for the TEM sample preparation. Therefore, in order to understand the effect of the diluted solution on the HAp porous body, the dimensional changes of the porous HAp green bodies after the TEM sample preparation were measured.

Table 3. Dimensional changes in the porous HAp green bodies just after removal from the mold subjected to the TEM sample preparation using a different solvent.

| Condition (Diluted solution) | As-prepared (Water) | As-prepared (Ethanol) |
|---|---|---|
| Size retention after the treatment (%) | 99.0 | 74.3 |

Table 3 shows the dimensional changes in the as-prepared porous HAp green bodies after the TEM sample preparation using different kinds of solvents. In the present study, the HAp porous green body in the as-prepared condition was chosen because the sample structure can be easily changed due to the high water content. In the case of the water treatment, only a 0.1 % shrinkage was observed. However, when treated using ethanol, the size retention of the HAp porous green body was 74.3 %. This result indicated that an approximately 25 %

Journal Name RSCPublishing

ARTICLE

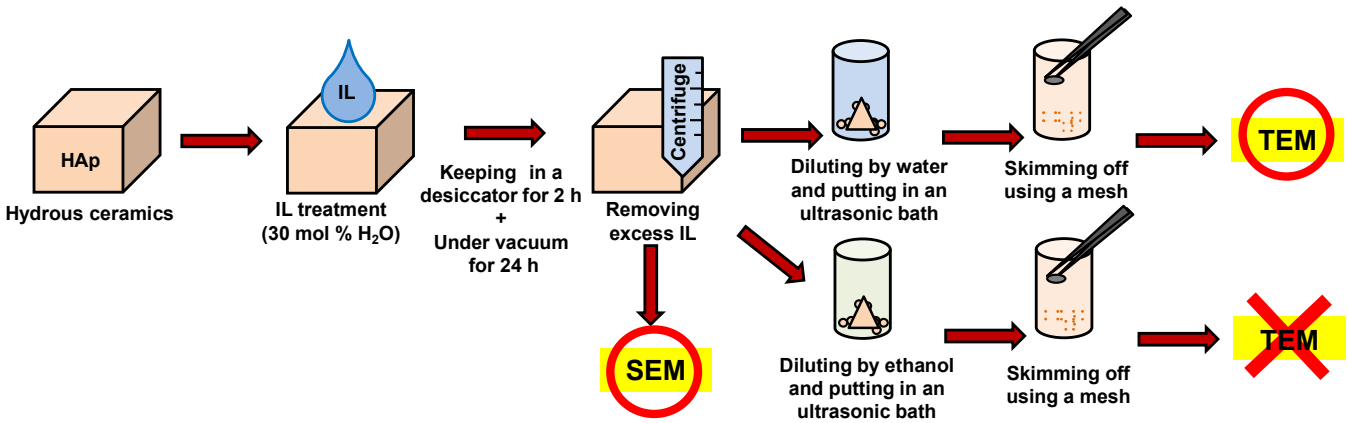


Fig. 6. Sample preparation method for microscopic observation of hydrous HAp green body using the IL.

volume shrinkage occured by the ethanol treatment. This indicated that ethanol affects the structure of the hydrous HAp porous body.

### 3.7. Estimation of microscopic observation method for hydrous HAp

A schematic outline was able to be proposed for the preparation method of the hydrated ceramic sample for the SEM and TEM observations and is shown in Figure 6.

From these studies, the following conclusions can be drawn. First, the hydrous HAp porous green bodies were treated with the raw IL. Thereby, the IL and water within the HAp sample displaced each other. In addition, the specific bonding between the IL and water, such as HOH$\cdots BF_4 \cdots$HOH, is helpful to maintain its original hydrous structure.[27] For the TEM observation, the HAp sample in the above condition needed to be diluted with a solvent before putting it in an ultrasonic bath. When the water as a diluted solution was applied to the HAp sample, the structure of the hydrous HAp porous green body can be observed. Although large amounts of water were added to the HAp porous green body treated with the IL, the structure of the HAp porous green body can be maintained without any drying. It is explained that the specific OH bonding cannot collapse due to the significant water treatment, because the specific bonding between the IL and water within a sample is quite strong.[33] On the other hand, when ethanol is used instead of water for the HAp sample, which was already treated by the IL, the structure of the hydrous HAp porous green body was changed. The ethanol affects the interaction between the IL and water within the HAp sample. Wu et al. reported that the addition of ethanol can break the strong interaction between the IL ([BMIM][$BF_4$]) and water.[34]

In the hydrous montmorillonite and IL intercalated montmorillonite case, the ethanol can be used for the TEM observation.[31] It is explained that the structure of the intercalated montmorillonite is stable due to its specific intercalation ability. Thereby, the structure of the intercalated montmorillonite was observed without any change though large amounts of ethanol were used for the TEM sample preparation.

## Conclusions

We established the optimized TEM observation method of a hydrous HAp green body by employing the hydrophilic IL. The crystal nanostructure of the hydrated HAp green body during the gelcasting process was successfully observed. The solvent effect on the observations of the nanostructural HAp green body was determined in order to develop the observation method using the IL. These results showed that water is a suitable solvent for the TEM sample preparation of the hydrous HAp green body. On the other hand, ethanol is not adequate as a solvent for the TEM observation. The solidification and calcination behaviors of the HAp particles during the gelcasting process were also revealed. This nano-scaled characterization of the hydrous ceramic green body has an advantage for the fabrication of advanced ceramic materials.

## Acknowledgements

The authors are grateful to Prof. H. Saka, of Nagoya University, Japan for useful discussions. CT would also like to thank Mr. T. Suzuki, of JEOL Co for his valuable help regarding the FFT analyses.

## Notes and references

*Advanced Ceramics Research Center, Nagoya Institute of Technology, 3-101-1, Honmachi, Tajimi, Gifu, 507-0033, Japan.*

Electronic Supplementary Information (ESI) available: [(1) Flow chart of gelcasting process, (2) TEM images of the HAp green body that has been stored in the humid chamber 90 to 50 % following the IL treatment using

water, (3) TEM images of as-prepared HAp green body after the TEM sample preparation using ethanol.].

1 I. Sopyan and J. Kaur, *Ceram. Int*., 2009, **35**, 3161–3168.
2 S. Padilla, J. Roman and M. Vallet-Regi, *J. Mater. Sci:Mater. Med*., 2002, **13**, 1193–1197.
3 C.J. Bae, H.W. Kim, Y.H. Koh and H.E. Kim, *J. Mater. Sci:Mater. Med*., 2006, **17**, 517–521.
4 W.Y. Zhou, S.H. Lee, M. Wang, W.L. Cheung and W.Y. Ip, *J. Mater. Sci:Mater. Med*., 2008, **19**, 2535–2540.
5 O.O. Omatete, M.A. Janney and R.A. Strehlow, Am. Ceram. Soc., Bull. 1991, **70**, 1641–1649.
6 O.O. Omatete, M.A. Janney and S.D. Nunn, *J. Euro. Ceram. Soc*., 1997, **17**, 407–413.
7 A.C. Young, O.O. Omatete, M.A. Janney and P.A. Menchhofer, *J. Am. Ceram. Soc*., 1991, **74**, 612–618.
8 J. Ma, Z. Xie, H. Miao, Y. Huang, Y. Cheng and W. Yang, *J. Euro. Ceram. Soc*., 2003, **23**, 2273–2279.
9 O.O. Omatete, J.P. Pollinger and K. O'Young, *Ceram. Trans*., 1995, **56**, 337–343.
10 L.G. Ma, Y. Huang, J.L. Yang, Z.P. Xie, X.L. Xu and J.S. Zhao, *J. Mater. Sci. Lett*., 2001, **20**, 1285–1288.
11 M.D. Vlajic and V. D. Krstic, *J. Mat. Sci*., 2002, **37**, 2943–2947.
12 Z.Z. Yi, Z.P. Xie, Y. Huang, J.T. Ma and Y.B. Cheng, *Ceram. Int*., 2002, **28**, 369–376.
13 X. Liu, Y. Huang and J. Yang, *Ceram. Int*., 2002, **28**, 59–164.
14 P. Sepulveda, J.G.P. Binner, S.O. Rogero, O.Z. Higa and J.C. Brsessiani, J. Biomed. Mater. Res., 2000, 50, 27–34.
15 D.J.A. Netz, P. Sepulveda, V.C. Pandolfelli, A.C.C. Spadaro, J.B. Alencastre, M.V.L.B. Bentley and J.M. Marchetti, *Inter. J. Pharm*., 2001, **213**, 117–125.
16 F. H. Hurley and T. P. Wier, *J. Electrochem. Soc*., 1951, **98**, 203–206.
17 J. S. Wilkes and M. J. Zaworotko, *J. Chem. Soc., Chem. Commun*., 1992, **13**, 965–967.
18 H. Li, P. S. Bhadury, B. Song and S. Yang, *RSC Adv*., 2012, **2**, 12525–12551.
19 S. Chen, L. Li, X. Wang, W. Tian, X. Wang, D.M. Tang, Y. Bando and D. Golberg, *Nanoscale*, 2012, **4**, 2658–2662.
20 K. Schütte, H. Meyer, C. Gemel, J. Barthel, R.A. Fischer and C. Janiak, *Nanoscale*, 2014, Advance Article.
21 T. Kakibe, J. Hishii, N. Yoshimoto, M. Egashira and M. Morita, *J. Power Sources*, 2012, **203**, 195–200.
22 K. Okazaki, T. Kiyama, K. Hirahara, N. Tanaka, S. Kuwabata and T. Torimoto, *Chem. Commun*., 2008, 691–693.
23 T. Torimoto, K. Okazaki, T. Kiyama, K. Hirahara, N. Tanaka and S. Kuwabata, *Appl. Phys. Lett*., 2006, **89**, 243117.
24 S. Kuwabata, T. Tsuda and T. Torimoto, *J. Phys. Chem. Lett*., 2010, **1**, 3177–3188.
25 S. Arimoto, M. Sugimura, H. Kageyama, T. Torimoto and S. Kuwabata, *Electrochim. Acta*., 2008, **53**, 6228–6234.
26 K. Kawai, K. Kaneko, H. Kawakami and T. Yonezawa, *Langmuir*, 2011, **27**, 9671–9675.
27 C. Takahashi, T. Shirai and M. Fuji, *Mater. Chem. Phys*., 2012, **133**, 565–572.
28 C. Takahashi, D. K. Pattanayak, T. Shirai and M. Fuji, *J. Euro. Ceram. Soc*., 2013, **33**, 629–635.
29 C. Takahashi, T. Shirai and M. Fuji, *Micros. Res. Tech*., 2012, **76**, 66–71.
30 C. Takahashi, T. Shirai and M. Fuji, *Mater. Chem. Phys*., 2012, **135**, 681–686.
31 C. Takahashi, T. Shirai and M. Fuji, *Mater. Chem. Phys*., 2013, **141**, 657–664.
32 C. Takahashi, D. K. Pattanayak, T. Shirai and M. Fuji, *Ceram. Int*., 2013, **39**, 1065–1073.
33 H. Abe, Y. Yoshimura, Y. Imai, T. Goto and H. Matsumoto, *J. Mol. Liquids*, 2009, **150**, 16–21.
34 B. Wu, Y. Zhang and H. Wang, *J. Phys. Chem*., 2009, **113**, 12332–12336.